

Dirichlet Extremals for Discrete Plateau Problems in GT–Bézier Spaces via PSO

Muhammad Ammad^{*1}, Md Yushalify Misro^{†2}, Samia Bibi², and Ahmad Ramli²

¹Department of Mathematics, Hong Kong Baptist University, Kowloon Tong, Hong Kong

²School of Mathematical Sciences, Universiti Sains Malaysia, 11800 Gelugor, Pulau Pinang, Malaysia

Abstract

We study a discrete analogue of the parametric Plateau problem in a non-polynomial tensor-product surface spaces generated by the generalized trigonometric (GT)–Bézier basis. Boundary interpolation is imposed by prescribing the boundary rows and columns of the control net, while the interior control points are selected by a Dirichlet principle: for each admissible choice of Bézier basis shape parameters, we compute the unique Dirichlet-energy extremal within the corresponding GT–Bézier patch space, which yields a parameter-dependent symmetric linear system for the interior control net under standard nondegeneracy assumptions. The remaining design freedom is thereby reduced to a four-parameter optimization problem, which we solve by particle swarm optimization. Numerical experiments show that the resulting two-level procedure consistently decreases the Dirichlet energy and, in our tests, often reduces the realized surface area relative to classical Bernstein–Bézier Dirichlet patches and representative quasi-harmonic and bending-energy constructions under identical boundary control data. We further adapt the same Dirichlet-extremal methodology to a hybrid tensor-product/bilinear Coons framework, obtaining minimality-biased TB–Coons patches from sparse boundary specifications.

Keywords: GT-Bézier surfaces, Plateau-GT-Bézier problem, Particle Swarm Optimization, Harmonic Bézier surfaces, Minimal surfaces, TB–Coons surfaces

1 Introduction

Minimal surfaces arise as stationary points of the area functional under fixed boundary data and occupy a central role in geometric analysis and its applications; see, e.g., [1–6]. Their ubiquity in capillarity and membrane equilibria motivates the continued study [7], while modern engineering and design, including architecture, materials, marine structures and bioinspired morphogenesis, often exploit their geometric efficiency [8, 9]. At smaller scales, periodic and bicontinuous configurations connect minimal surface theory to nanostructuring and molecular engineering [10].

Let $D \subset \mathbb{R}^2$ be a bounded simply connected Lipschitz domain. Given a rectifiable Jordan curve $\Gamma \subset \mathbb{R}^3$ and a continuous weakly monotone parametrization $\gamma : \partial D \rightarrow \Gamma$, consider maps $S \in W^{1,2}(D; \mathbb{R}^3)$ with trace $S|_{\partial D} = \gamma$. Writing

$$G_S := (\nabla S)^\top \nabla S \quad \text{and} \quad J_S := \sqrt{\det G_S},$$

^{*}Corresponding author: 21481199@life.hkbu.edu.hk

[†]E-mail: yushalify@usm.my

the (parametric) Plateau problem may be expressed as

$$\inf \left\{ \mathcal{A}[S] : S \in W^{1,2}(D; \mathbb{R}^3), S|_{\partial D} = \gamma \right\}, \quad \mathcal{A}[S] := \int_D J_S \, dx. \quad (1.1)$$

For smooth immersions, criticality of \mathcal{A} is equivalent to vanishing mean curvature. Direct minimization of \mathcal{A} over parametrizations is analytically delicate due to reparametrization invariance and degenerating minimizing sequences. Following Douglas' harmonic relaxation [11], modern approaches to this problem include [12] for theoretical aspects and [13] for computational implementations.

$$\mathcal{D}[S] := \frac{1}{2} \int_D \text{tr}(G_S) \, dx = \frac{1}{2} \int_D (\|\partial_1 S\|^2 + \|\partial_2 S\|^2) \, dx. \quad (1.2)$$

The pointwise arithmetic–geometric mean inequality yields

$$J_S = \sqrt{\det G_S} \leq \frac{1}{2} \text{tr}(G_S) \quad \text{a.e. on } D, \quad \text{hence} \quad \mathcal{A}[S] \leq \mathcal{D}[S].$$

Moreover, equality holds if and only if S is conformal (isothermal), i.e.

$$\langle \partial_1 S, \partial_2 S \rangle = 0 \quad \text{and} \quad \|\partial_1 S\| = \|\partial_2 S\| \quad \text{a.e. on } D,$$

so that Dirichlet minimizers in a conformal gauge recover minimal surfaces [14].

In geometric modeling one replaces the infinite-dimensional admissible class by a finite-dimensional ansatz. The classical “Plateau–Bézier problem” [15, 16] restricts S to tensor-product Bézier patches with boundary control points fixed to interpolate prescribed curves. Although the inequality $\mathcal{A} \leq \mathcal{D}$ does not, in general, yield a rigorous comparison of discrete minimizers (since conformality is not enforced within a fixed discrete space), Dirichlet extremals are known to provide reliable approximations of area extremals in many practical settings [2, 15]. Closely related discretizations employ finite elements and variational formulations [17], multiresolution B-spline schemes leading to sparse linear systems for near-minimal surfaces [18], and analyses of Dirichlet-type energies in polyhedral settings [19]; see also modern discrete differential geometry and geometry-processing treatments connecting conformal parameterization, Laplacians, and energy minimization [20–22]. Additional strands include quasi-harmonic constructions in non-polynomial spaces [16], low-subdivision modeling [23], explicit low-degree polynomial minimal patches [24, 25], geodesically constrained approximations [26], and canonical factor formulations for minimal surface equations [27]. Variational area-reduction flows within parametric classes have also been explored [28].

In this work we adopt the GT-Bézier basis [29], a generalized trigonometric–Bézier system of degree ≥ 2 enjoying partition-of-unity, nonnegativity, and symmetry properties analogous to the Bernstein basis, while introducing two shape parameters per univariate direction. Henceforth, we specialize in the parametric domain $D = [0, 1]^2$, and encode the boundary condition by fixing boundary control rows and columns to interpolate the prescribed boundary curves. Let

$$\{G_{i,m}(\cdot; (\alpha_1, \alpha_2))\}_{i=0}^m, \quad \{G_{j,n}(\cdot; (\beta_1, \beta_2))\}_{j=0}^n$$

denote the GT-Bézier basis families in the u - and v -directions, respectively. A GT-Bézier tensor-product patch of bidegree (m, n) is

$$S_{m,n}(u, v; \boldsymbol{\alpha}, \mathbf{P}) = \sum_{i=0}^m \sum_{j=0}^n P_{i,j} G_{i,m}(u; (\alpha_1, \alpha_2)) G_{j,n}(v; (\beta_1, \beta_2)), \quad (u, v) \in [0, 1]^2, \quad (1.3)$$

where $\mathbf{P} = \{P_{i,j}\}_{0 \leq i \leq m, 0 \leq j \leq n} \subset \mathbb{R}^3$ is the control net. The boundary control points $\{P_{i,j}\}$ with $i \in \{0, m\}$ or $j \in \{0, n\}$ are prescribed by the boundary interpolation constraints, whereas the interior control points

$$\mathbf{p} := \{P_{i,j}\}_{1 \leq i \leq m-1, 1 \leq j \leq n-1} \in \mathbb{R}^{3(m-1)(n-1)}$$

remain unknown. The shape-parameter vector is

$$\boldsymbol{\alpha} := (\alpha_1, \alpha_2, \beta_1, \beta_2) \in \mathcal{P} \subset \mathbb{R}^4, \quad (1.4)$$

where \mathcal{P} is an admissible parameter set chosen so that the GT-Bézier basis is well-defined and retains its shape-preserving properties. In particular, letting $\Theta \subset \mathbb{R}^2$ denote the admissible univariate parameter set for the GT-Bézier basis (cf. Section 2), we assume

$$\mathcal{P} \subseteq \Theta \times \Theta. \quad (1.5)$$

For each fixed $\boldsymbol{\alpha} \in \mathcal{P}$, consider the discrete admissible class

$$\mathcal{S}_{m,n}(\boldsymbol{\alpha}) := \left\{ S_{m,n}(\cdot, \cdot; \boldsymbol{\alpha}, \mathbf{P}) : \mathbf{P} \text{ satisfies the boundary interpolation constraints} \right\}.$$

We define the discrete Dirichlet extremal (indeed, minimizer in the typical strictly convex case) by

$$S^*(\boldsymbol{\alpha}) \in \arg \min \{ \mathcal{D}[S] : S \in \mathcal{S}_{m,n}(\boldsymbol{\alpha}) \}. \quad (1.6)$$

Taking variations supported on interior degrees of freedom yields the normal equations: for each interior index pair $(k, \ell) \in \{1, \dots, m-1\} \times \{1, \dots, n-1\}$ and each component $a \in \{1, 2, 3\}$, let

$$\Phi_{k,\ell,a}(u, v) := G_{k,m}(u; (\alpha_1, \alpha_2)) G_{\ell,n}(v; (\beta_1, \beta_2)) e_a,$$

so that $\Phi_{k,\ell,a}|_{\partial([0,1]^2)} = 0$. Then the first variation of \mathcal{D} at $S^*(\boldsymbol{\alpha})$ yields

$$\int_{[0,1]^2} \langle \nabla S^*(\boldsymbol{\alpha}), \nabla \Phi_{k,\ell,a} \rangle \, du \, dv = 0. \quad (1.7)$$

Equivalently, the interior control vector $\mathbf{p} = \mathbf{p}(\boldsymbol{\alpha})$ satisfies a parameter-dependent linear system

$$A(\boldsymbol{\alpha}) \mathbf{p}(\boldsymbol{\alpha}) = \mathbf{b}(\boldsymbol{\alpha}), \quad (1.8)$$

where $A(\boldsymbol{\alpha})$ and $\mathbf{b}(\boldsymbol{\alpha})$ are determined explicitly by the GT-Bézier basis functions and their derivatives and by the fixed boundary control data. On the admissible set \mathcal{P} we assume $A(\boldsymbol{\alpha})$ is nonsingular, so that

$$\mathbf{p}(\boldsymbol{\alpha}) = A(\boldsymbol{\alpha})^{-1} \mathbf{b}(\boldsymbol{\alpha})$$

is well-defined.

We then introduce the reduced Dirichlet functional

$$\mathcal{J} : \mathcal{P} \rightarrow \mathbb{R}, \quad \mathcal{J}(\boldsymbol{\alpha}) := \mathcal{D}[S^*(\boldsymbol{\alpha})] = \mathcal{D}[S_{m,n}(\cdot, \cdot; \boldsymbol{\alpha}, \mathbf{P}(\boldsymbol{\alpha}))], \quad (1.9)$$

where $\mathbf{P}(\boldsymbol{\alpha})$ denotes the full control net obtained by combining the fixed boundary control points with the interior solution $\mathbf{p}(\boldsymbol{\alpha})$. We minimize \mathcal{J} over \mathcal{P} using particle swarm optimization (PSO), a widely used derivative-free metaheuristic; see, e.g., [30, 31].

$$\boldsymbol{\alpha}^* \in \arg \min_{\boldsymbol{\alpha} \in \mathcal{P}} \mathcal{J}(\boldsymbol{\alpha}).$$

In each evaluation of \mathcal{J} , the dependence on $\boldsymbol{\alpha}$ enters solely through the GT-Bézier basis (and its derivatives) and the solution of (1.8); no a priori numerical specialization of $\boldsymbol{\alpha}$ is required at the level of the variational formulation.

This construction retains the established strengths of Dirichlet extremals for Plateau–Bézier-type problems [2, 14, 32] while using the additional geometric degrees of freedom afforded by the GT-Bézier basis [29]. In practice, these shape parameters often permit lower Dirichlet energies than classical polynomial tensor-product Bézier patches under identical boundary data; empirically, this frequently correlates with reduced realized surface area. We further investigate the harmonic subclass of GT-Bézier patches, its dependence on boundary rows and columns, and its relationship to minimality in free-boundary regimes, connecting with harmonic parametrizations and discrete minimal surface literature [16, 19, 33, 34]. As an application, we employ the same Dirichlet-extremal principle to infer interior control points for TB–Coons blends, producing minimality-biased GT–Coons surfaces from parsimonious control specifications.

Section 2 recalls definitions and basic properties of classical and GT-Bézier surfaces. Section 3 formulates the Dirichlet-extremal construction for GT-Bézier patches and the associated reduced functional. Section 4 presents the particle swarm optimization procedure used to minimize \mathcal{J} , together with an explicit algorithm. Section 5 reports numerical examples for the Plateau–GT-Bézier problem. Section 6 discusses the relationship between minimal surfaces and harmonic surfaces in our framework. Section 7 applies the Dirichlet-extremal method in the trigonometric basis to construct minimal TB–Coons surfaces. Finally, Section 8 summarizes conclusions and future directions.

2 Preliminaries: GT-Bézier basis functions and shape-parameter effects

We recall the classical Bernstein basis and the generalized trigonometric (GT)-Bézier basis of Ammad et al. [29], adopting notation consistent with Section 1. Unless stated otherwise, the univariate parameter is $t \in [0, 1]$. For the GT-Bézier basis we use a univariate shape-parameter pair

$$\boldsymbol{\theta} := (\theta_1, \theta_2) \in \Theta \subset \mathbb{R}^2, \quad \Theta := [0.5, 3.5]^2,$$

thereby avoiding collision with the surface shape vector $\boldsymbol{\alpha} = (\alpha_1, \alpha_2, \beta_1, \beta_2) \in \mathcal{P} \subset \mathbb{R}^4$ introduced in Section 1. In view of (1.5), each tensor-product patch uses the two instantiated pairs

$$\boldsymbol{\alpha}^{(u)} = (\alpha_1, \alpha_2) \in \Theta, \quad \boldsymbol{\alpha}^{(v)} = (\beta_1, \beta_2) \in \Theta.$$

2.1 Bernstein polynomials and Bézier representation

Definition 1 (Bernstein polynomials [35, 36, Ch. 1]). Let $d \in \mathbb{N}_0$. For each $i = 0, \dots, d$, the i th Bernstein polynomial of degree d on $[0, 1]$ is defined by

$$B_{i,d}(t) := \binom{d}{i} t^i (1-t)^{d-i}, \quad t \in [0, 1]. \quad (2.1)$$

The collection $\{B_{i,d}\}_{i=0}^d$ is called the Bernstein basis of degree d on $[0, 1]$.

Definition 2 (Bézier curve [37]). Let $c_0, \dots, c_d \in \mathbb{R}^m$ (typically $m \in \{2, 3\}$) be control points. The (parametric) Bézier curve of degree d associated with $\{c_i\}_{i=0}^d$ is the map $C : [0, 1] \rightarrow \mathbb{R}^m$ given by

$$C(t) := \sum_{i=0}^d c_i B_{i,d}(t), \quad t \in [0, 1], \quad (2.2)$$

where $B_{i,d}$ are the Bernstein polynomials from Definition 1.

2.2 GT-Bézier basis: base case and degree elevation

Definition 3 (Quadratic GT-Bézier (base case)). Fix $\boldsymbol{\theta} = (\theta_1, \theta_2) \in \Theta$. The quadratic GT-Bézier basis on $[0, 1]$ is defined by

$$\begin{aligned} G_{0,2}(t; \boldsymbol{\theta}) &= \frac{\theta_1}{2} \left(\sin^2\left(\frac{\pi}{2}t\right) - \sin\left(\frac{\pi}{2}t\right) \right) + \cos^2\left(\frac{\pi}{2}t\right), \\ G_{2,2}(t; \boldsymbol{\theta}) &= \frac{\theta_2}{2} \left(\cos^2\left(\frac{\pi}{2}t\right) - \cos\left(\frac{\pi}{2}t\right) \right) + \sin^2\left(\frac{\pi}{2}t\right), \\ G_{1,2}(t; \boldsymbol{\theta}) &= 1 - G_{0,2}(t; \boldsymbol{\theta}) - G_{2,2}(t; \boldsymbol{\theta}). \end{aligned} \quad (2.3)$$

Definition 4 (Recursive degree elevation (GT-Bézier basis of degree $n \geq 3$)). For $n \geq 3$ and $k = 0, \dots, n$, define

$$G_{k,n}(t; \boldsymbol{\theta}) = (1-t)G_{k,n-1}(t; \boldsymbol{\theta}) + tG_{k-1,n-1}(t; \boldsymbol{\theta}), \quad (2.4)$$

with the convention $G_{k,n} \equiv 0$ whenever $k < 0$ or $k > n$. The family $\{G_{k,n}(\cdot; \boldsymbol{\theta})\}_{k=0}^n$ is called the GT-Bézier basis of degree n associated with the seed (2.3); cf. [29].

Proposition 2.1 (Partition of unity and endpoint interpolation). For each $n \geq 2$ and $\boldsymbol{\theta} \in \Theta$,

$$\sum_{k=0}^n G_{k,n}(t; \boldsymbol{\theta}) = 1 \quad \text{for all } t \in [0, 1],$$

and

$$G_{0,n}(0; \boldsymbol{\theta}) = 1, \quad G_{n,n}(1; \boldsymbol{\theta}) = 1, \quad G_{k,n}(0; \boldsymbol{\theta}) = G_{k,n}(1; \boldsymbol{\theta}) = 0 \quad (k \notin \{0, n\}).$$

Proof. The endpoint identities follow from the explicit seed (2.3) and the recursion (2.4) by induction on n . The partition-of-unity property is verified for $n = 2$ from (2.3) and is propagated to $n \geq 3$ by summing (2.4) over k and using the induction hypothesis. \square

Remark 2.1 (Link to the surface parameters of Section 1). In the bivariate setting (1.3), we employ two independent GT families:

$$\{G_{i,m}(\cdot; \boldsymbol{\alpha}^{(u)})\}_{i=0}^m \text{ in the } u\text{-direction,} \quad \{G_{j,n}(\cdot; \boldsymbol{\alpha}^{(v)})\}_{j=0}^n \text{ in the } v\text{-direction.}$$

Thus the univariate shape-pair $\boldsymbol{\theta}$ used in this section is instantiated as $\boldsymbol{\theta} = \boldsymbol{\alpha}^{(u)}$ (respectively $\boldsymbol{\alpha}^{(v)}$) when constructing the tensor-product patch.

2.3 Influence of Shape Parameters on GT-Bézier Curves

Definition 5 (Univariate GT-Bézier curve). Given control points $\{b_k\}_{k=0}^n \subset \mathbb{R}^m$ ($m \in \{2, 3\}$), degree $n \geq 2$, and the GT-Bézier basis $\{G_{k,n}(\cdot; \boldsymbol{\theta})\}_{k=0}^n$, the associated GT-Bézier curve is

$$F(t; \boldsymbol{\theta}) = \sum_{k=0}^n G_{k,n}(t; \boldsymbol{\theta}) b_k, \quad t \in [0, 1]. \quad (2.5)$$

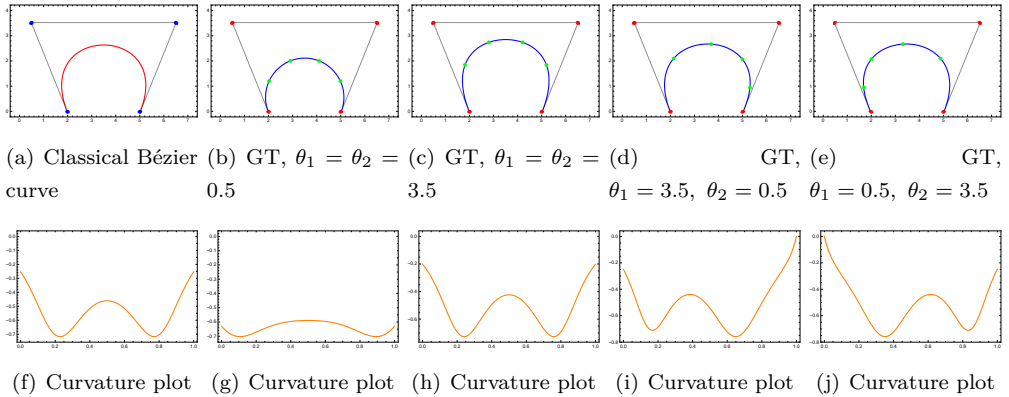


Figure 1: Cubic GT-Bézier curves and corresponding curvature plots under varying shape parameters.

Curvature diagnostics. Curvature plots are a standard diagnostic for shape regularity in geometric design. Restricting to planar curves $F(\cdot; \boldsymbol{\theta}) \subset \mathbb{R}^2$, suppose $F \in C^2([0, 1]; \mathbb{R}^2)$ is regular, i.e. $F'(t) \neq 0$ for all t . Its signed curvature is

$$\kappa_{F(\cdot; \boldsymbol{\theta})}(t) = \frac{\det(F'(t; \boldsymbol{\theta}), F''(t; \boldsymbol{\theta}))}{\|F'(t; \boldsymbol{\theta})\|^3}, \quad t \in [0, 1]. \quad (2.6)$$

In particular, the dependence of the curvature on the shape parameters may be regarded as the nonlinear operator

$$\mathcal{K} : \Theta \rightarrow L^\infty(0, 1), \quad \mathcal{K}(\boldsymbol{\theta}) := \kappa_{F(\cdot; \boldsymbol{\theta})}(\cdot),$$

whose nontriviality stems from the trigonometric seed (2.3) and its propagation through the recursion (2.4). Empirically, varying $\boldsymbol{\theta}$ redistributes parametric stretch along t , thereby shifting the location and magnitude of curvature extrema while preserving endpoint interpolation (Proposition 2.1) and the affine-combination structure of (2.5). When, additionally, nonnegativity holds for the chosen admissible set Θ (as in [29]), the curve remains within the convex hull of its control polygon.

Figure 1 illustrates representative cubic GT-Bézier curves under different parameter selections alongside their curvature plots, demonstrating modulation of curvature magnitude and its spatial allocation induced by the shape variables.

3 Extremals of the Dirichlet functional for GT-Bézier surfaces

We work on $D = [0, 1]^2$ and consider GT-Bézier surfaces $S_{m,n}(\cdot, \cdot; \boldsymbol{\alpha}, \mathbf{P})$ with fixed boundary control rows and columns. In this section we express the condition that a GT-Bézier surface is an extremal of the Dirichlet functional (with prescribed boundary) as an explicit linear system in the interior control points. Rather than deriving the Euler–Lagrange equation in a strong form, we view the Dirichlet energy as a real-valued function on the Euclidean space of interior control variables and characterize its critical points by vanishing of the gradient. Closed-form recursive formulas for the derivatives of the GT-Bézier basis, used to evaluate the integrals appearing below, are provided in Appendix A.

3.1 Tensor-product GT-Bézier surface and Dirichlet functional

Let $m, n \geq 2$ and let $\boldsymbol{\alpha} = (\alpha_1, \alpha_2, \beta_1, \beta_2) \in \mathcal{P}$ be the surface shape vector. For notational convenience we set

$$\boldsymbol{\alpha}^{(u)} := (\alpha_1, \alpha_2) \in \Theta, \quad \boldsymbol{\alpha}^{(v)} := (\beta_1, \beta_2) \in \Theta. \quad (3.1)$$

We denote the corresponding GT-Bézier basis by $G_{i,m}(u; \boldsymbol{\alpha}^{(u)})$ and $G_{j,n}(v; \boldsymbol{\alpha}^{(v)})$. Given control points $\{P_{ij}\}_{i,j=0}^{m,n} \subset \mathbb{R}^3$, define the GT-Bézier tensor-product surface

$$S(u, v; \boldsymbol{\alpha}, \mathbf{P}) = \sum_{i=0}^m \sum_{j=0}^n P_{ij} G_{i,m}(u; \boldsymbol{\alpha}^{(u)}) G_{j,n}(v; \boldsymbol{\alpha}^{(v)}), \quad (u, v) \in [0, 1]^2. \quad (3.2)$$

Its Dirichlet functional is

$$\mathcal{D}[S] := \frac{1}{2} \int_0^1 \int_0^1 \left(\|S_u(u, v)\|^2 + \|S_v(u, v)\|^2 \right) du dv. \quad (3.3)$$

3.2 Extremal condition as a linear system in the control points

Theorem 1 (Dirichlet extremals for GT-Bézier surfaces). Let S be the GT-Bézier surface (3.2) with prescribed boundary control points $\{P_{ij} : i \in \{0, m\} \text{ or } j \in \{0, n\}\}$. Then S is an extremal of the Dirichlet functional (3.3) (with respect to variations of the interior control points) if and only if, for every $k \in \{1, \dots, m-1\}$, $\ell \in \{1, \dots, n-1\}$, and each $\mu \in \{1, 2, 3\}$,

$$\begin{aligned} \sum_{i=0}^{m-1} \sum_{j=0}^n I_{k,i}^{(1)} J_{\ell,j}^{(1)} \langle e^\mu, P_{i+1,j} - P_{i,j} \rangle + \sum_{i=0}^{m-1} \sum_{j=0}^n I_{k,i}^{(2)} J_{\ell,j}^{(1)} \langle e^\mu, P_{i,j} \rangle \\ + \sum_{i=0}^m \sum_{j=0}^{n-1} I_{k,i}^{(3)} J_{\ell,j}^{(2)} \langle e^\mu, P_{i,j+1} - P_{i,j} \rangle + \sum_{i=0}^m \sum_{j=0}^{n-1} I_{k,i}^{(3)} J_{\ell,j}^{(3)} \langle e^\mu, P_{i,j} \rangle = 0. \end{aligned} \quad (3.4)$$

Here e^μ denotes the μ -th canonical basis vector of \mathbb{R}^3 and $\langle \cdot, \cdot \rangle$ is the Euclidean inner product. The scalar coefficients are

$$I_{k,i}^{(1)} := \int_0^1 G'_{k,m}(u; \boldsymbol{\alpha}^{(u)}) \left(G_{i,m-1}(u; \boldsymbol{\alpha}^{(u)}) + u G'_{i,m-1}(u; \boldsymbol{\alpha}^{(u)}) \right) du, \quad (3.5)$$

$$I_{k,i}^{(2)} := \int_0^1 G'_{k,m}(u; \boldsymbol{\alpha}^{(u)}) G'_{i,m-1}(u; \boldsymbol{\alpha}^{(u)}) du, \quad (3.6)$$

$$I_{k,i}^{(3)} := \int_0^1 G_{k,m}(u; \boldsymbol{\alpha}^{(u)}) G_{i,m}(u; \boldsymbol{\alpha}^{(u)}) du, \quad (3.7)$$

$$J_{\ell,j}^{(1)} := \int_0^1 G_{\ell,n}(v; \boldsymbol{\alpha}^{(v)}) G_{j,n}(v; \boldsymbol{\alpha}^{(v)}) dv, \quad (3.8)$$

$$J_{\ell,j}^{(2)} := \int_0^1 G'_{\ell,n}(v; \boldsymbol{\alpha}^{(v)}) \left(G_{j,n-1}(v; \boldsymbol{\alpha}^{(v)}) + v G'_{j,n-1}(v; \boldsymbol{\alpha}^{(v)}) \right) dv, \quad (3.9)$$

$$J_{\ell,j}^{(3)} := \int_0^1 G'_{\ell,n}(v; \boldsymbol{\alpha}^{(v)}) G'_{j,n-1}(v; \boldsymbol{\alpha}^{(v)}) dv. \quad (3.10)$$

Proof. Write each control point as $P_{ij} = (x_{ij}^1, x_{ij}^2, x_{ij}^3) \in \mathbb{R}^3$. For fixed (k, ℓ) with $1 \leq k \leq m-1$, $1 \leq \ell \leq n-1$ and $\mu \in \{1, 2, 3\}$, consider the partial derivative $\partial \mathcal{D}[S] / \partial x_{k\ell}^\mu$. Using the standard identity (e.g., [2])

$$\frac{\partial \mathcal{D}[S]}{\partial x_{k\ell}^\mu} = \int_0^1 \int_0^1 \left(\left\langle S_u, \frac{\partial S_u}{\partial x_{k\ell}^\mu} \right\rangle + \left\langle S_v, \frac{\partial S_v}{\partial x_{k\ell}^\mu} \right\rangle \right) du dv,$$

it remains to compute S_u , S_v , and the variations $\partial S_u / \partial x_{k\ell}^\mu$, $\partial S_v / \partial x_{k\ell}^\mu$.

From (3.2),

$$\frac{\partial S}{\partial x_{k\ell}^\mu}(u, v) = G_{k,m}(u; \boldsymbol{\alpha}^{(u)}) G_{\ell,n}(v; \boldsymbol{\alpha}^{(v)}) e^\mu,$$

hence by commuting partial derivatives,

$$\frac{\partial S_u}{\partial x_{k\ell}^\mu}(u, v) = G'_{k,m}(u; \boldsymbol{\alpha}^{(u)}) G_{\ell,n}(v; \boldsymbol{\alpha}^{(v)}) e^\mu, \quad \frac{\partial S_v}{\partial x_{k\ell}^\mu}(u, v) = G_{k,m}(u; \boldsymbol{\alpha}^{(u)}) G'_{\ell,n}(v; \boldsymbol{\alpha}^{(v)}) e^\mu.$$

Next, we use the derivative representation of the GT-Bézier surface (cf. the formulas collected in Appendix A) to write

$$\begin{aligned} S_u(u, v) &= \sum_{i=0}^{m-1} \sum_{j=0}^n \left(G_{i,m-1}(u; \boldsymbol{\alpha}^{(u)}) + u G'_{i,m-1}(u; \boldsymbol{\alpha}^{(u)}) \right) G_{j,n}(v; \boldsymbol{\alpha}^{(v)}) (P_{i+1,j} - P_{i,j}) \\ &\quad + \sum_{i=0}^{m-1} \sum_{j=0}^n G'_{i,m-1}(u; \boldsymbol{\alpha}^{(u)}) G_{j,n}(v; \boldsymbol{\alpha}^{(v)}) P_{i,j}, \\ S_v(u, v) &= \sum_{i=0}^m \sum_{j=0}^{n-1} G_{i,m}(u; \boldsymbol{\alpha}^{(u)}) \left(G_{j,n-1}(v; \boldsymbol{\alpha}^{(v)}) + v G'_{j,n-1}(v; \boldsymbol{\alpha}^{(v)}) \right) (P_{i,j+1} - P_{i,j}) \\ &\quad + \sum_{i=0}^m \sum_{j=0}^{n-1} G_{i,m}(u; \boldsymbol{\alpha}^{(u)}) G'_{j,n-1}(v; \boldsymbol{\alpha}^{(v)}) P_{i,j}. \end{aligned}$$

Substituting these expressions into the gradient formula and using bilinearity of $\langle \cdot, \cdot \rangle$ gives

$$\begin{aligned} \frac{\partial \mathcal{D}[S]}{\partial x_{k\ell}^\mu} &= \sum_{i=0}^{m-1} \sum_{j=0}^n \langle e^\mu, P_{i+1,j} - P_{i,j} \rangle \int_0^1 \int_0^1 G'_{k,m}(u; \boldsymbol{\alpha}^{(u)}) \left(G_{i,m-1}(u; \boldsymbol{\alpha}^{(u)}) + u G'_{i,m-1}(u; \boldsymbol{\alpha}^{(u)}) \right) \\ &\quad \times G_{\ell,n}(v; \boldsymbol{\alpha}^{(v)}) G_{j,n}(v; \boldsymbol{\alpha}^{(v)}) du dv \\ &\quad + \sum_{i=0}^{m-1} \sum_{j=0}^n \langle e^\mu, P_{i,j} \rangle \int_0^1 \int_0^1 G'_{k,m}(u; \boldsymbol{\alpha}^{(u)}) G'_{i,m-1}(u; \boldsymbol{\alpha}^{(u)}) G_{\ell,n}(v; \boldsymbol{\alpha}^{(v)}) G_{j,n}(v; \boldsymbol{\alpha}^{(v)}) du dv \\ &\quad + \sum_{i=0}^m \sum_{j=0}^{n-1} \langle e^\mu, P_{i,j+1} - P_{i,j} \rangle \int_0^1 \int_0^1 G_{k,m}(u; \boldsymbol{\alpha}^{(u)}) G_{i,m}(u; \boldsymbol{\alpha}^{(u)}) \\ &\quad \times G'_{\ell,n}(v; \boldsymbol{\alpha}^{(v)}) \left(G_{j,n-1}(v; \boldsymbol{\alpha}^{(v)}) + v G'_{j,n-1}(v; \boldsymbol{\alpha}^{(v)}) \right) du dv \\ &\quad + \sum_{i=0}^m \sum_{j=0}^{n-1} \langle e^\mu, P_{i,j} \rangle \int_0^1 \int_0^1 G_{k,m}(u; \boldsymbol{\alpha}^{(u)}) G_{i,m}(u; \boldsymbol{\alpha}^{(u)}) G'_{\ell,n}(v; \boldsymbol{\alpha}^{(v)}) G'_{j,n-1}(v; \boldsymbol{\alpha}^{(v)}) du dv. \end{aligned}$$

Finally, each double integral separates into a product of a u -integral and a v -integral, yielding precisely the coefficients (3.5)–(3.8). Therefore $\partial \mathcal{D}[S] / \partial x_{k\ell}^\mu = 0$ for all interior indices (k, ℓ) and components μ is equivalent to (3.4), completing the proof. \square

Equation (3.4) is the coordinate form of the weak normal equations (1.7) from Section 1 restricted to the GT-Bézier tensor-product space. Upon ordering the interior control variables into the vector $\mathbf{p} \in \mathbb{R}^{3(m-1)(n-1)}$, the collection of equations (3.4) assembles into the linear system $A(\boldsymbol{\alpha})\mathbf{p} = \mathbf{b}(\boldsymbol{\alpha})$ in (1.8), where the entries of $A(\boldsymbol{\alpha})$ and $\mathbf{b}(\boldsymbol{\alpha})$ are determined by the coefficients (3.5)–(3.8) and by the prescribed boundary control data.

By Theorem 1, prescribing the boundary control points and taking the interior control points $\{P_{k\ell}\}_{k,\ell}^{m-1,n-1}$ as unknowns yields a square linear system (3.4). Whenever the associated coefficient matrix is nonsingular (equivalently, the stiffness matrix is positive definite on the interior degrees of freedom), this system has a unique solution, hence a unique Dirichlet extremal in the chosen GT-Bézier tensor-product space.

We now connect this Dirichlet-based discretization with the geometric goal of minimizing area. For smooth charts, the Dirichlet energy dominates the area functional and agrees with it exactly for conformal (in particular, isothermal) parametrizations. The next theorem shows that, assuming the existence of an isothermal area-minimizing chart and sufficiently dense boundary sampling, the areas of the resulting GT-Dirichlet extremals admit an asymptotic upper bound in terms of the minimal area.

Theorem 2 (Asymptotic upper bound for the area of GT-Dirichlet extremals). Let $S : [0, 1]^2 \rightarrow \mathbb{R}^3$ be a C^2 immersion which is an isothermal parametrization. For each $d \in \mathbb{N}$, let Y_d be the GT-Bézier surface of degree (d, d) (with fixed shape parameters $\alpha \in \mathcal{P}$) which minimizes the Dirichlet functional among all GT-Bézier surfaces whose boundary control points coincide with the sampled boundary net

$$P_d = \left\{ S\left(\frac{i}{d}, \frac{j}{d}\right) \right\}_{i,j=0}^d \quad \text{on } \partial\{0, \dots, d\}^2.$$

Assume moreover that there exists a sequence of GT-Bézier surfaces X_d of degree (d, d) with the same boundary data P_d such that $X_d \rightarrow S$ in $C^1([0, 1]^2)$ as $d \rightarrow \infty$. Then

$$\lim_{d \rightarrow \infty} \mathcal{A}[X_d] = \mathcal{A}[S] \quad \text{and} \quad \limsup_{d \rightarrow \infty} \mathcal{A}[Y_d] \leq \mathcal{A}[S],$$

where $\mathcal{A}[\cdot]$ denotes the area functional.

Proof. We use three standard ingredients.

(i) Area is bounded by Dirichlet energy. For any C^1 map $F : [0, 1]^2 \rightarrow \mathbb{R}^3$, the arithmetic-geometric mean inequality yields

$$\|F_u\|^2 + \|F_v\|^2 \geq 2\|F_u\| \|F_v\| \geq 2\|F_u \times F_v\|.$$

Integrating gives

$$\mathcal{A}[F] = \int_{[0,1]^2} \|F_u \times F_v\| \leq \frac{1}{2} \int_{[0,1]^2} (\|F_u\|^2 + \|F_v\|^2) = \mathcal{D}[F]. \quad (3.11)$$

(ii) Equality for isothermal parametrizations. Since S is isothermal, we have $\langle S_u, S_v \rangle = 0$ and $\|S_u\| = \|S_v\|$ on $[0, 1]^2$. Hence $\|S_u \times S_v\| = \|S_u\| \|S_v\| = \|S_u\|^2 = \frac{1}{2}(\|S_u\|^2 + \|S_v\|^2)$, and therefore

$$\mathcal{A}[S] = \mathcal{D}[S]. \quad (3.12)$$

(iii) Minimality of Y_d for the Dirichlet energy under the discrete boundary constraint. By construction, Y_d minimizes $\mathcal{D}[\cdot]$ over the affine subspace of GT charts with boundary control points fixed by P_d . In particular, for any admissible competitor F in the same GT-Bézier space with the same boundary data,

$$\mathcal{D}[Y_d] \leq \mathcal{D}[F]. \quad (3.13)$$

Now fix d and take as competitor $F = X_d$, which is admissible by hypothesis (same boundary net P_d). Combining (3.11) and (3.13) yields

$$\mathcal{A}[Y_d] \leq \mathcal{D}[Y_d] \leq \mathcal{D}[X_d].$$

Since $X_d \rightarrow S$ in $C^1([0, 1]^2)$, we have $X_{d,u} \rightarrow S_u$ and $X_{d,v} \rightarrow S_v$ uniformly; hence $\mathcal{D}[X_d] \rightarrow \mathcal{D}[S]$. Using (3.12), we conclude

$$\limsup_{d \rightarrow \infty} \mathcal{A}[Y_d] \leq \lim_{d \rightarrow \infty} \mathcal{D}[X_d] = \mathcal{D}[S] = \mathcal{A}[S].$$

Finally, $\mathcal{A}[X_d] \rightarrow \mathcal{A}[S]$ follows directly from the C^1 convergence and continuity of the area integrand $\|F_u \times F_v\|$ under uniform convergence of F_u, F_v . \square

Remark 3.1. The conclusion is stated as a \limsup because the discrete boundary constraint fixes only a sampled boundary net, so Y_d need not span the same Jordan curve Γ for each d . If one enforces exact boundary interpolation $Y_d|_{\partial D} = S|_{\partial D}$ (or assumes an appropriate stability result under boundary perturbations), the \limsup can be strengthened to a full limit.

4 Optimization of the reduced Dirichlet functional via Particle Swarm Optimization

We consider the reduced Dirichlet functional $\mathcal{J}(\boldsymbol{\alpha}) = \mathcal{D}[S^*(\boldsymbol{\alpha})]$, where $S^*(\boldsymbol{\alpha})$ is the GT–Dirichlet extremal obtained by solving the interior-control linear system (1.8) for fixed $\boldsymbol{\alpha} = (\alpha_1, \alpha_2, \beta_1, \beta_2) \in \mathcal{P}$. In this section we describe the numerical strategy used to minimize \mathcal{J} over the admissible parameter set \mathcal{P} , namely particle swarm optimization (PSO) [38, 39].

Let $\mathcal{P} \subseteq \Theta \times \Theta$ be the admissible set for the GT-Bézier basis shape parameters (cf. (1.4)–(1.5)). The optimization problem was solved in the numerical experiments are

$$\boldsymbol{\alpha}^* \in \arg \min_{\boldsymbol{\alpha} \in \mathcal{P}} \mathcal{J}(\boldsymbol{\alpha}), \quad \mathcal{J}(\boldsymbol{\alpha}) := \mathcal{D}[S^*(\boldsymbol{\alpha})], \quad (4.1)$$

where, for each $\boldsymbol{\alpha} \in \mathcal{P}$, the surface $S^*(\boldsymbol{\alpha})$ is the unique Dirichlet extremal in the GT-Bézier tensor-product space with the prescribed boundary control net, obtained by solving

$$A(\boldsymbol{\alpha}) \mathbf{p}(\boldsymbol{\alpha}) = \mathbf{b}(\boldsymbol{\alpha}). \quad (4.2)$$

4.1 Particle Swarm Optimization (PSO)

PSO is a population-based stochastic metaheuristic inspired by collective motion such as bird flocking [40, 41]. It maintains a set (swarm) of N particles, each representing a candidate position vector

$$x_i(t) \in \mathbb{R}^D, \quad D = 4,$$

where we identify $x_i = (\alpha_1, \alpha_2, \beta_1, \beta_2)$ and enforce the bound constraints $x_i(t) \in \mathcal{P}$ (e.g. via clamping or projection). At iteration t , each particle has a velocity $v_i(t) \in \mathbb{R}^D$, a personal best position $x_i^b(t)$ (the best position it has visited so far), and the swarm shares a global best position $x_g^b(t)$ (the best across all particles). With i.i.d. random vectors $r_1(t), r_2(t) \in [0, 1]^D$, the global-best PSO update is

$$\begin{cases} v_i(t) = w v_i(t-1) + c_1 r_1(t) \odot (x_g^b(t-1) - x_i(t-1)) + c_2 r_2(t) \odot (x_i^b(t-1) - x_i(t-1)), \\ x_i(t) = x_i(t-1) + v_i(t), \end{cases} \quad (4.3)$$

where \odot denotes componentwise multiplication. The inertia weight w controls momentum (exploration vs. exploitation), and $c_1, c_2 > 0$ are acceleration (learning) parameters weighting the global (social) and

personal (cognitive) terms, respectively. In our implementation, after the position update we enforce feasibility $x_i(t) \in \mathcal{P}$ and then re-evaluate the fitness $f(x_i(t)) := \mathcal{J}(x_i(t))$.

Local-best variant. A common alternative replaces the global best x_g^b by a neighborhood best x_i^b computed over a prescribed neighborhood of particle i . This can enhance exploration and reduce premature convergence, at the cost of slower convergence rates. In this work we use the global-best variant (4.3) unless otherwise stated.

In our setting the PSO objective is the reduced Dirichlet functional (4.1), i.e.

$$\min_{\boldsymbol{\alpha} \in \mathcal{P}} f(\boldsymbol{\alpha}) = \min_{\boldsymbol{\alpha} \in \mathcal{P}} \mathcal{J}(\boldsymbol{\alpha}) = \min_{\boldsymbol{\alpha} \in \mathcal{P}} \frac{1}{2} \int_{[0,1]^2} \left(\|S_u^*(\boldsymbol{\alpha})\|^2 + \|S_v^*(\boldsymbol{\alpha})\|^2 \right) du dv. \quad (4.4)$$

Equivalently, one may write $S^*(\boldsymbol{\alpha}) = S_{m,n}(\cdot, \cdot; \boldsymbol{\alpha}, \mathbf{P}(\boldsymbol{\alpha}))$ with $\mathbf{P}(\boldsymbol{\alpha})$ obtained from (4.2). Algorithm 1 summarizes the PSO procedure used in the numerical experiments.

Unless otherwise specified, we use a swarm size $N = 50$, inertia weight $w = 0.7$, and acceleration coefficients $c_1 = c_2 = 1.5$. Each particle is initialized as a 4-vector $\boldsymbol{\alpha}_i(0) = (\alpha_1, \alpha_2, \beta_1, \beta_2) \in \mathcal{P}$ (uniformly at random within the bounds of \mathcal{P}), and velocities are initialized uniformly in a symmetric range

Algorithm 1 Particle Swarm Optimization (PSO) for minimizing $\mathcal{J}(\boldsymbol{\alpha})$

Require: Objective $f(\boldsymbol{\alpha}) = \mathcal{J}(\boldsymbol{\alpha})$, admissible set \mathcal{P} , dimension $D = 4$, swarm size N , max iterations T_{\max} , parameters w, c_1, c_2

Ensure: Best parameters $\boldsymbol{\alpha}_g^b$ and value $f(\boldsymbol{\alpha}_g^b)$

- 1: Initialize particles $\boldsymbol{\alpha}_i(0) \in \mathcal{P}$ (e.g. uniform in bounds), $i = 1, \dots, N$
- 2: Initialize velocities $v_i(0)$ (e.g. uniform in a symmetric box), $i = 1, \dots, N$
- 3: Set personal bests $\boldsymbol{\alpha}_i^b(0) = \boldsymbol{\alpha}_i(0)$ and evaluate $f(\boldsymbol{\alpha}_i^b(0))$
- 4: Set global best $\boldsymbol{\alpha}_g^b(0) \in \arg \min_i f(\boldsymbol{\alpha}_i^b(0))$
- 5: for $t = 1$ to T_{\max} do
- 6: for $i = 1$ to N do
- 7: Draw $r_1, r_2 \sim U([0, 1]^D)$
- 8: Update velocity: $v_i(t) = w v_i(t-1) + c_1 r_1 \odot (\boldsymbol{\alpha}_g^b(t-1) - \boldsymbol{\alpha}_i(t-1)) + c_2 r_2 \odot (\boldsymbol{\alpha}_i^b(t-1) - \boldsymbol{\alpha}_i(t-1))$
- 9: Update position: $\boldsymbol{\alpha}_i(t) = \boldsymbol{\alpha}_i(t-1) + v_i(t)$
- 10: Enforce bounds: project/clamp $\boldsymbol{\alpha}_i(t)$ onto \mathcal{P}
- 11: Evaluate fitness $f(\boldsymbol{\alpha}_i(t))$
- 12: if $f(\boldsymbol{\alpha}_i(t)) < f(\boldsymbol{\alpha}_i^b(t-1))$ then
- 13: $\boldsymbol{\alpha}_i^b(t) = \boldsymbol{\alpha}_i(t)$
- 14: if $f(\boldsymbol{\alpha}_i^b(t)) < f(\boldsymbol{\alpha}_g^b(t-1))$ then
- 15: $\boldsymbol{\alpha}_g^b(t) = \boldsymbol{\alpha}_i^b(t)$
- 16: end if
- 17: else
- 18: $\boldsymbol{\alpha}_i^b(t) = \boldsymbol{\alpha}_i^b(t-1)$
- 19: end if
- 20: end for
- 21: end for
- 22: return $\boldsymbol{\alpha}_g^b(T_{\max}), f(\boldsymbol{\alpha}_g^b(T_{\max}))$

proportional to the parameter box size. The global-best variant (4.3) is employed.

5 Numerical examples: Plateau problem for GT–Bézier patches via Dirichlet extremals

In this section we report numerical experiments for the (discrete) Plateau problem in the class of GT–Bézier tensor-product patches. Throughout, the boundary control net is prescribed, and the unknown interior control points are computed as the Dirichlet extremal in the chosen finite-dimensional GT–Bézier space (Section 3, cf. (1.8)). In addition, the shape-parameter vector $\boldsymbol{\alpha} = (\alpha_1, \alpha_2, \beta_1, \beta_2) \in \mathcal{P}$ is selected by minimizing the reduced Dirichlet energy

$$\mathcal{J}(\boldsymbol{\alpha}) = \mathcal{D}[S^*(\boldsymbol{\alpha})], \quad \boldsymbol{\alpha}^* \in \arg \min_{\boldsymbol{\alpha} \in \mathcal{P}} \mathcal{J}(\boldsymbol{\alpha}),$$

where $S^*(\boldsymbol{\alpha})$ denotes the GT–Dirichlet extremal surface for the fixed boundary data at parameter $\boldsymbol{\alpha}$ (Section 4). Hence each evaluation $\mathcal{J}(\boldsymbol{\alpha})$ requires solving the interior linear system and then computing \mathcal{D} (numerically) on $[0, 1]^2$.

For comparison we also construct: (i) the classical Bernstein–Bézier Dirichlet patch [2], (ii) the quasi-harmonic surface [16], and (iii) the bending-energy surface [42]. All surfaces share the same boundary control points. We visualize the resulting patches and, in addition, we display mean-curvature nephograms. For a smooth minimal surface the mean curvature H vanishes identically; in discrete or constrained settings one typically expects H to be small rather than exactly zero [15].

Example 5.1 (Bicubic boundary net I). Let $\{P_{ij}\}_{i,j=0}^3 \subset \mathbb{R}^3$ be a 4×4 bicubic control net whose boundary points are fixed as

$$\begin{aligned} P_{0,0} &= (0, 0, 0), & P_{0,1} &= (2, 0, 2), & P_{0,2} &= (4, 0, -2), & P_{0,3} &= (6, 0, 0), \\ P_{1,0} &= (0, 2, 2), & P_{1,3} &= (6, 2, 2), \\ P_{2,0} &= (0, 4, -2), & P_{2,3} &= (6, 4, -2), \\ P_{3,0} &= (0, 6, 2), & P_{3,1} &= (2, 6, 2), & P_{3,2} &= (4, 6, -2), & P_{3,3} &= (6, 6, 0). \end{aligned}$$

For each admissible shape-parameter vector $\boldsymbol{\alpha} = (\alpha_1, \alpha_2, \beta_1, \beta_2) \in \mathcal{P}$, let $S^*(\cdot, \cdot; \boldsymbol{\alpha})$ denote the GT–Bézier patch whose boundary control points are as above and whose interior control points are chosen as the Dirichlet extremal, i.e. obtained from (1.8). The numerical Plateau problem in this GT–Bézier class is then the reduced optimization problem

$$\boldsymbol{\alpha}^* \in \arg \min_{\boldsymbol{\alpha} \in \mathcal{P}} \mathcal{J}(\boldsymbol{\alpha}) = \arg \min_{\boldsymbol{\alpha} \in \mathcal{P}} \mathcal{D}[S^*(\boldsymbol{\alpha})].$$

We solve this problem by PSO as described in Section 4. The resulting surface (with the optimized shape parameters) is shown in Figure 2(a). The competing surfaces obtained by the Bernstein–Bézier Dirichlet method, the quasi-harmonic method, and the bending-energy method are shown in Figure 2(b)–(d). The PSO convergence histories (10 independent runs) are shown in Figure 4(a).

Example 5.2 (Bicubic boundary net II). Let the boundary control points of a bicubic net $\{P_{ij}\}_{i,j=0}^3$ be

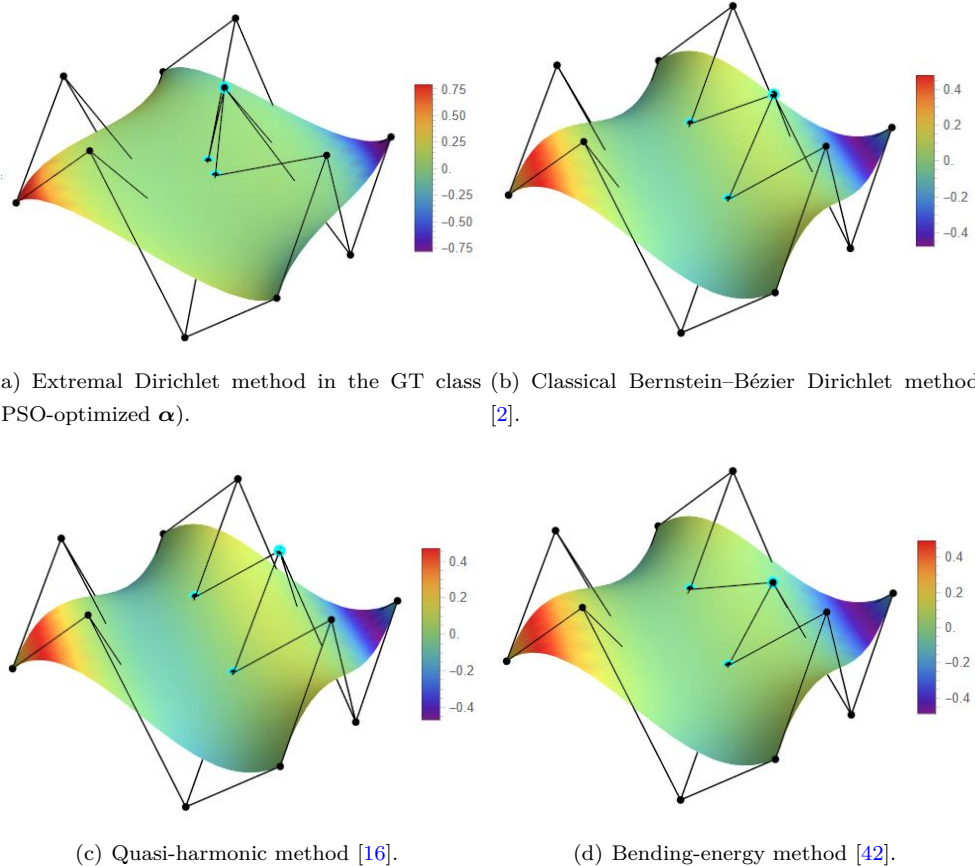


Figure 2: Bicubic surfaces constructed from the same boundary control points by different approaches.

prescribed by

$$\begin{aligned}
 P_{0,0} &= (0, 0, 0), & P_{0,1} &= (2, 0, 2), & P_{0,2} &= (4, 0, 2), & P_{0,3} &= (6, 0, 0), \\
 P_{1,0} &= (0, 2, 2), & P_{1,3} &= (6, 2, 2), \\
 P_{2,0} &= (0, 4, 2), & P_{2,3} &= (6, 4, 2), \\
 P_{3,0} &= (0, 6, 2), & P_{3,1} &= (2, 6, 2), & P_{3,2} &= (4, 6, 2), & P_{3,3} &= (6, 6, 0).
 \end{aligned}$$

As in Example 5.1, for each $\alpha \in \mathcal{P}$ we compute the interior control points as the GT–Dirichlet extremal and minimize the reduced functional $\mathcal{J}(\alpha)$ by PSO. The resulting GT surface is displayed in Figure 3(a), together with the comparison methods in Figure 3(b)–(d). The convergence histories for 10 runs are shown in Figure 4(b). In particular, the proposed method yields a surface with small mean curvature magnitudes (nearly harmonic behavior) while achieving the lowest surface area/Dirichlet energy among the tested methods for this boundary configuration.

To quantify the comparison, Table 1 reports the attained surface areas (computed from the resulting parametric surfaces) together with the optimized shape parameters for the proposed method. In both examples the PSO-optimized GT–Dirichlet extremal yields the smallest area among the tested approaches, indicating that the added shape degrees of freedom (optimized at the energy level) effectively improve the quality of the discrete Plateau solution within the chosen finite-dimensional ansatz space.

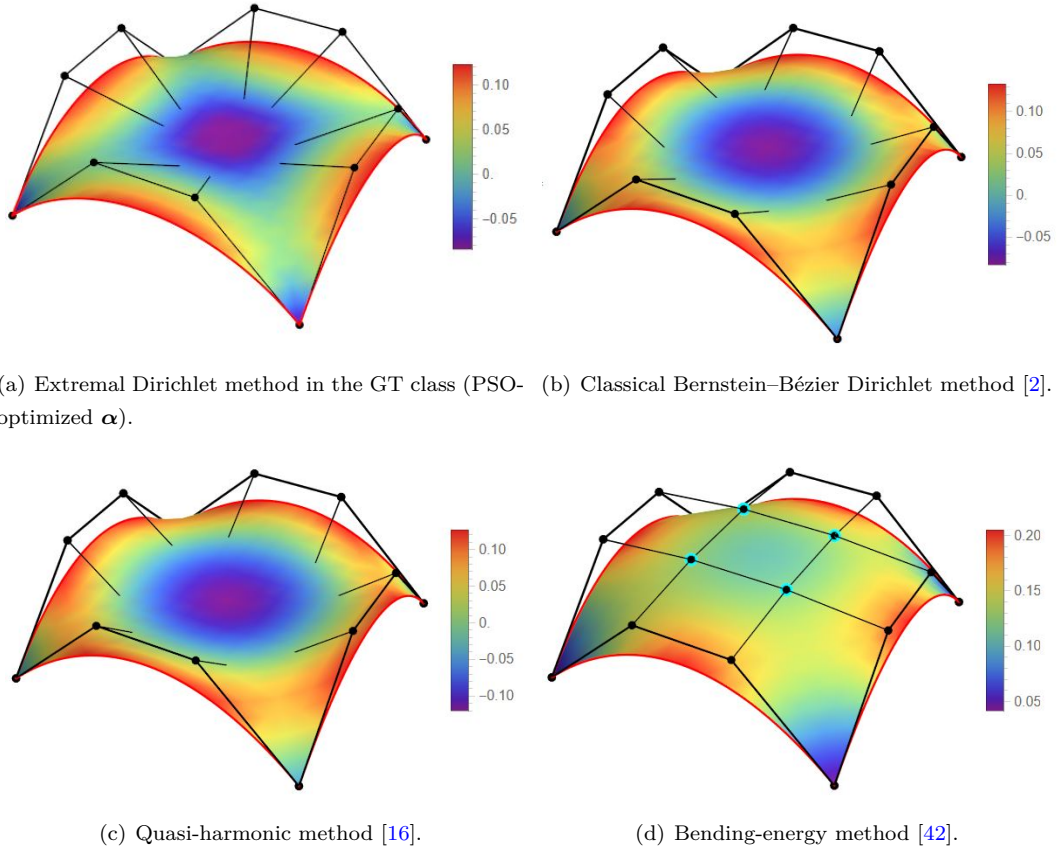


Figure 3: Bicubic surfaces constructed from the same boundary control points by different approaches.

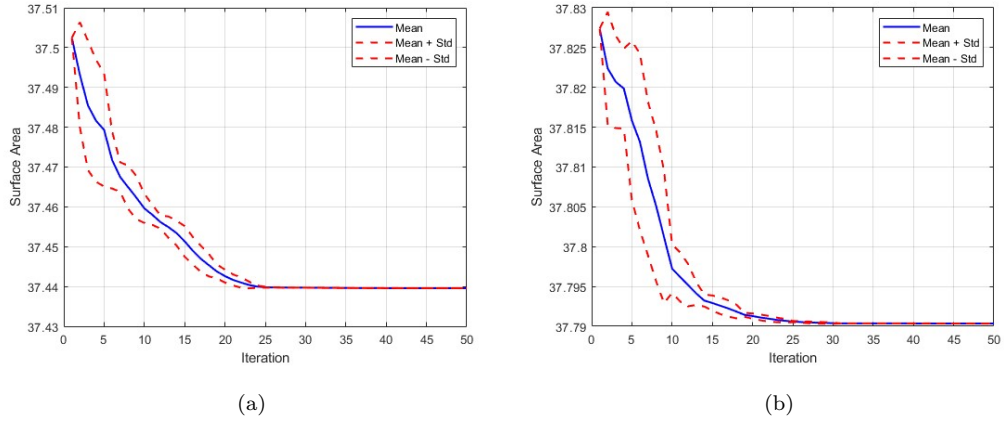


Figure 4: PSO convergence histories for minimizing $\mathcal{J}(\alpha)$ (10 runs): (a) Example 5.1; (b) Example 5.2.

Table 1: Surface-area comparison for Examples 5.1 and 5.2.

| Method | Example 5.1 | | Example 5.2 | |
|--|-----------------|-------------------|---|-------------------|
| | Area | Shape parameters | Area | Shape parameters |
| PSO-based Dirichlet (proposed) | GT– extremal | 37.4396 0.8706 | $\alpha_1 = \alpha_2 = \beta_1 = \beta_2 =$ 0.8706 | 37.7905 1.4823 |
| Bernstein–Bézier Dirichlet method [2] | | 38.0000 | N/A | 38.0000 |
| Quasi-harmonic method [16] | | 38.3817 | N/A | 38.0826 |
| Bending-energy method [42] | | 38.4057 | N/A | 40.0661 |

6 Relation to harmonic patches

Let $D = [0, 1]^2$ be the parameter domain. For a sufficiently smooth parametric surface $S \in H^1(D; \mathbb{R}^3)$, the Dirichlet functional is

$$\mathcal{D}(S) = \frac{1}{2} \int_D \left(\|S_u\|^2 + \|S_v\|^2 \right) du dv. \quad (6.1)$$

In the unconstrained (infinite-dimensional) setting, where S ranges over all admissible maps with fixed boundary trace $S|_{\partial D}$ —the Euler–Lagrange equation associated with (6.1) is the vector Laplace equation

$$\Delta S = S_{uu} + S_{vv} = 0 \quad \text{in } D, \quad (6.2)$$

so that the minimizer is harmonic. Denote this unconstrained minimizer by S^{harm} .

In the constrained (finite-dimensional) setting of this paper, S is restricted to the GT–Bézier tensor-product space with prescribed boundary control points (and, for each fixed $\boldsymbol{\alpha} = (\alpha_1, \alpha_2, \beta_1, \beta_2) \in \mathcal{P}$, the interior control points are chosen as the Dirichlet extremal in that space). Let S^{GT} be the resulting constrained minimizer for the same boundary data. Since the admissible class is smaller, the variational inequality

$$\mathcal{D}(S^{\text{harm}}) \leq \mathcal{D}(S^{\text{GT}}) \quad (6.3)$$

holds, with strict inequality in general. Equality can occur only if the constrained patch happens to satisfy (6.2), i.e. it is harmonic in the classical sense.

6.1 Constructing (approximately) harmonic GT–Bézier surfaces

Because a generic GT–Bézier patch does not satisfy $\Delta S \equiv 0$ identically, we measure harmonicity by the least-squares Laplacian defect

$$\mathcal{F}(\boldsymbol{\alpha}) = \int_D \|\Delta S(u, v; \boldsymbol{\alpha})\|^2 du dv, \quad \boldsymbol{\alpha} = (\alpha_1, \alpha_2, \beta_1, \beta_2) \in \mathcal{P}, \quad (6.4)$$

and select $\boldsymbol{\alpha}$ by minimizing \mathcal{F} (using PSO as in Section 4). Here $S(\cdot, \cdot; \boldsymbol{\alpha})$ is the GT-Bézier surface constructed from a control net whose missing points are first computed from a discrete harmonicity condition at the control-net level, following [15].

Let $\tilde{S}(u, v) = \sum_{i=0}^n \sum_{j=0}^m B_i^n(u) B_j^m(v) P_{ij}$ be a classical tensor-product Bézier surface. Using standard second-difference operators

$$\Delta^{2,0} P_{ij} = P_{i+2,j} - 2P_{i+1,j} + P_{i,j}, \quad \Delta^{0,2} P_{ij} = P_{i,j+2} - 2P_{i,j+1} + P_{i,j},$$

one can express $\Delta \tilde{S}$ in a Bernstein basis of degree (n, m) and obtain, for interior indices (i, j) , a linear relation of the form (see [15])

$$\begin{aligned} n(n-1) & \left(a_{i,n} \Delta^{2,0} P_{ij} + b_{i-1,n} \Delta^{2,0} P_{i-1,j} + c_{i-2,n} \Delta^{2,0} P_{i-2,j} \right) \\ & + m(m-1) \left(a_{j,m} \Delta^{0,2} P_{ij} + b_{j-1,m} \Delta^{0,2} P_{i,j-1} + c_{j-2,m} \Delta^{0,2} P_{i,j-2} \right) = 0, \end{aligned} \quad (6.5)$$

where, for $k \in \{0, \dots, n-2\}$,

$$a_{k,n} = (n-k)(n-k-1), \quad b_{k,n} = 2(k+1)(n-k-1), \quad c_{k,n} = (k+1)(k+2),$$

and similarly for $(a_{k,m}, b_{k,m}, c_{k,m})$. Given partial boundary data, (6.5) yields a linear system for the missing control points of a harmonic (Bernstein) patch.

After computing the missing control points by (6.5) (in the Bernstein setting), we construct a GT-Bézier patch with the same control net and then tune $\boldsymbol{\alpha}$ by minimizing the harmonicity defect (6.4). This yields a GT patch with ΔS small in the L^2 sense, hence ‘‘approximately harmonic’’ in the variational sense.

Remark 6.1. Classical Bézier patches admit harmonic constructions through linear constraints on the control net, but they lack the additional shape degrees of freedom inherent to the GT-Bézier basis. The GT-Bézier basis parameters provide an extra level of geometric control: they can be selected to (i) reduce the harmonicity defect (6.4) and/or (ii) subsequently reduce the Dirichlet energy (or area) while maintaining the same boundary data.

Example 6.1 (Harmonic reconstruction from partial boundary data). We consider two configurations of missing data. In Case 1, only the first and last columns of the control net are prescribed (Figure 5(a)); in Case 2, only the first and last rows are prescribed (Figure 5(c)). In each case we compute the remaining control points by solving the linear system induced by (6.5). We then construct the corresponding GT-Bézier patch and optimize the shape parameters $\boldsymbol{\alpha} \in \mathcal{P}$ by minimizing the harmonicity defect $\mathcal{F}(\boldsymbol{\alpha})$ in (6.4) via PSO. The resulting approximately harmonic GT-Bézier surfaces and their curvature nephograms are shown in Figure 5(b),(d). The PSO convergence history (10 runs) is reported in Figure 6.

7 Extremals of the Dirichlet functional and minimal TB-Coons surfaces

Let $D = [0, 1]^2$ be the parameter domain. Given four boundary curves

$$\Gamma_0(u), \Gamma_1(u) \quad (u \in [0, 1]), \quad \Gamma_2(v), \Gamma_3(v) \quad (v \in [0, 1]),$$

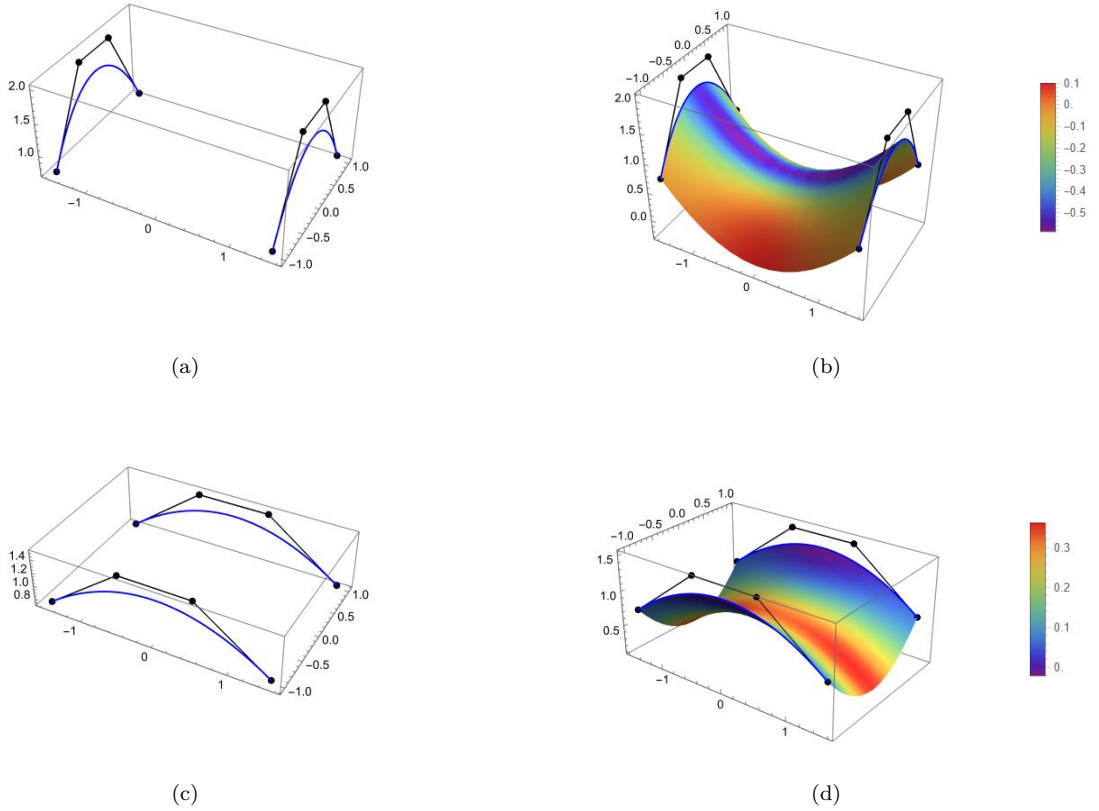


Figure 5: Approximately harmonic GT–Bézier surfaces from partial boundary control data.

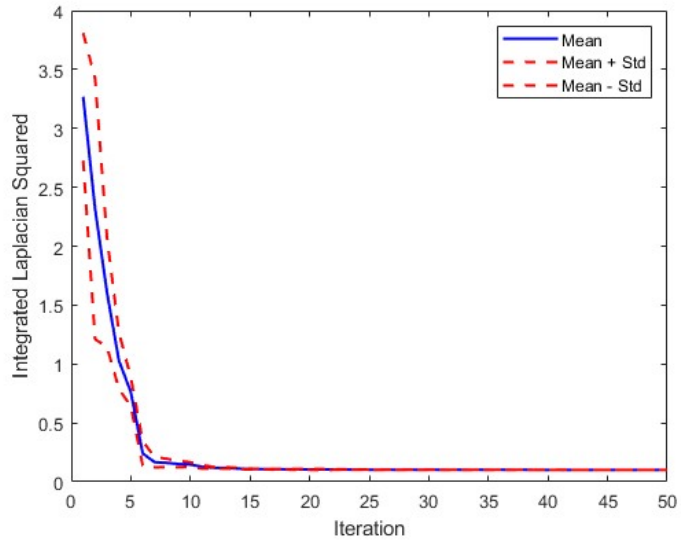


Figure 6: PSO convergence for minimizing the harmonicity defect $\mathcal{F}(\boldsymbol{\alpha})$ in (6.4).

satisfying the standard vertex compatibility conditions

$$\Gamma_0(0) = \Gamma_2(0), \quad \Gamma_0(1) = \Gamma_3(0), \quad \Gamma_1(0) = \Gamma_2(1), \quad \Gamma_1(1) = \Gamma_3(1),$$

the classical bilinearly blended Coons patch is the interpolant $\tilde{S} : D \rightarrow \mathbb{R}^3$ defined by

$$\tilde{S}(u, v) = (1 - v)\Gamma_0(u) + v\Gamma_1(u) + (1 - u)\Gamma_2(v) + u\Gamma_3(v) - \tilde{S}_{\text{bil}}(u, v), \quad (7.1)$$

where the bilinear corner correction is

$$\tilde{S}_{\text{bil}}(u, v) = (1 - u)(1 - v)C_{00} + (1 - u)vC_{01} + u(1 - v)C_{10} + uvC_{11}, \quad (7.2)$$

with $C_{00} = \Gamma_0(0)$, $C_{01} = \Gamma_0(1)$, $C_{10} = \Gamma_1(0)$, $C_{11} = \Gamma_1(1)$. Equivalently, (7.1) can be written in the compact matrix form

$$\tilde{S}(u, v) = - \begin{bmatrix} -1 & 1 - u & u \end{bmatrix} \begin{bmatrix} 0 & \Gamma_0(u) & \Gamma_1(u) \\ \Gamma_2(v) & C_{00} & C_{01} \\ \Gamma_3(v) & C_{10} & C_{11} \end{bmatrix} \begin{bmatrix} -1 \\ 1 - v \\ v \end{bmatrix}. \quad (7.3)$$

Throughout, we use the standard linear blending functions

$$h_0(u) = 1 - u, \quad h_1(u) = u, \quad g_0(v) = 1 - v, \quad g_1(v) = v,$$

so that (7.3) matches the usual Coons construction.

Assume that the four boundary curves are represented by cubic control polygons. Using the notation of previous sections, let $\{B_{i,3}\}_{i=0}^3$ denote the classical Bernstein basis and let $\{G_{i,3}(\cdot; \boldsymbol{\alpha})\}_{i=0}^3$ denote the cubic GT-Bézier basis, with parameter vector $\boldsymbol{\alpha} = (\alpha_1, \alpha_2, \beta_1, \beta_2) \in \mathcal{P}$ (the same admissible set \mathcal{P} used in Section 4). Let $\{Q_{ij}\}_{i,j=0}^3 \subset \mathbb{R}^3$ be the 4×4 control net, where the twelve boundary points are prescribed and the four interior points $Q_{11}, Q_{12}, Q_{21}, Q_{22}$ are unknown. We represent the u -boundary curves by cubic Bernstein polynomials

$$\Gamma_k(u) = \sum_{i=0}^3 B_{i,3}(u) Q_{k,i}, \quad k \in \{0, 3\}, \quad u \in [0, 1], \quad (7.4)$$

and the v -boundary curves similarly as

$$\Gamma_\ell(v) = \sum_{j=0}^3 B_{j,3}(v) Q_{j,\ell}, \quad \ell \in \{0, 3\}, \quad v \in [0, 1], \quad (7.5)$$

where the index placement is chosen to be consistent with the tensor-product net $\{Q_{ij}\}$ (corners are $Q_{00}, Q_{03}, Q_{30}, Q_{33}$). The Bernstein basis functions $B_{i,3}$ are as in (2.1). (Compared to the earlier discussion, we avoid mixing m, n with a fixed cubic degree, and we correct the index mismatch.)

We now introduce two tensor-product patches that share the same control net $\{Q_{ij}\}$ but use mixed basis.

(i) Bernstein in u and GT-Bézier in v . Define

$$R_1(u, v; \boldsymbol{\alpha}) = \sum_{i=0}^3 \sum_{j=0}^3 B_{i,3}(u) G_{j,3}(v; \boldsymbol{\alpha}) Q_{ij}. \quad (7.6)$$

Then the boundary curves $v = 0$ and $v = 1$ interpolate the Bernstein curves determined by the first and last rows $\{Q_{i0}\}_{i=0}^3$ and $\{Q_{i3}\}_{i=0}^3$, while $u = 0, 1$ are GT-Bézier curves in v .

(ii) GT–Bézier in u and Bernstein in v . Similarly,

$$R_2(u, v; \boldsymbol{\alpha}) = \sum_{i=0}^3 \sum_{j=0}^3 G_{i,3}(u; \boldsymbol{\alpha}) B_{j,3}(v) Q_{ij}. \quad (7.7)$$

Construct the four GT boundary curves (degree 3) induced by the same boundary control points:

$$\Gamma'_k(u; \boldsymbol{\alpha}) = \sum_{i=0}^3 G_{i,3}(u; \boldsymbol{\alpha}) Q_{k,i}, \quad k \in \{0, 3\}, \quad (7.8)$$

$$\Gamma'_\ell(v; \boldsymbol{\alpha}) = \sum_{j=0}^3 G_{j,3}(v; \boldsymbol{\alpha}) Q_{j,\ell}, \quad \ell \in \{0, 3\}. \quad (7.9)$$

Using these four GT curves in the bilinear Coons blending, define the GT–Coons corner correction patch

$$T(u, v; \boldsymbol{\alpha}) = - \begin{bmatrix} 0 & \Gamma'_0(u; \boldsymbol{\alpha}) & \Gamma'_3(u; \boldsymbol{\alpha}) \\ \Gamma'_0(v; \boldsymbol{\alpha}) & Q_{00} & Q_{03} \\ \Gamma'_3(v; \boldsymbol{\alpha}) & Q_{30} & Q_{33} \end{bmatrix} \begin{bmatrix} -1 \\ 1 - v \\ v \end{bmatrix}. \quad (7.10)$$

By construction, T coincides with the same corner data and removes the double-counting of the bilinear part in the standard Coons decomposition.

We define the TB–Coons surface (tensor-product Bernstein/GT hybrid with Coons correction) by

$$\mathcal{S}(u, v; \boldsymbol{\alpha}) = R_1(u, v; \boldsymbol{\alpha}) + R_2(u, v; \boldsymbol{\alpha}) - T(u, v; \boldsymbol{\alpha}). \quad (7.11)$$

The surface \mathcal{S} interpolates the prescribed boundary curves in the sense inherited from (7.6)–(7.10). The construction is illustrated in Fig. 7. The remaining degrees of freedom are precisely the four interior control points $Q_{11}, Q_{12}, Q_{21}, Q_{22}$ (and, if desired, the shape parameters $\boldsymbol{\alpha}$).

To impose minimality, we minimize the Dirichlet energy on D :

$$\mathcal{D}(\mathcal{S}(\cdot, \cdot; \boldsymbol{\alpha})) = \frac{1}{2} \int_D \left(\|\partial_u \mathcal{S}(u, v; \boldsymbol{\alpha})\|^2 + \|\partial_v \mathcal{S}(u, v; \boldsymbol{\alpha})\|^2 \right) du dv, \quad (7.12)$$

subject to fixed boundary control points. In the unconstrained setting, the minimizer with fixed boundary trace is harmonic (and, under conformality, minimal). Here, however, we restrict to the finite-dimensional TB–Coons ansatz (7.11); thus the computed patch is a Dirichlet extremal within the TB–Coons space, i.e. the Galerkin projection of the harmonic map onto the span of the chosen basis.

For each fixed $\boldsymbol{\alpha} \in \mathcal{P}$, the functional (7.12) is a quadratic form in the unknown interior control points. Consequently, the necessary and sufficient optimality condition is the linear system

$$\nabla_{(Q_{11}, Q_{12}, Q_{21}, Q_{22})} \mathcal{D}(\mathcal{S}(\cdot, \cdot; \boldsymbol{\alpha})) = 0, \quad (7.13)$$

which yields the unique interior control points provided the associated stiffness matrix is positive definite (which holds under the standard nondegeneracy assumptions on the basis). We additionally optimize $\boldsymbol{\alpha}$ over \mathcal{P} using PSO as in Section 4, i.e.

$$\boldsymbol{\alpha}^* \in \arg \min_{\boldsymbol{\alpha} \in \mathcal{P}} \mathcal{D}(\mathcal{S}(\cdot, \cdot; \boldsymbol{\alpha})), \quad (7.14)$$

where for each particle position $\boldsymbol{\alpha}$ the interior points are computed from (7.13). We call the resulting surface $\mathcal{S}(\cdot, \cdot; \boldsymbol{\alpha}^*)$ a minimal TB–Coons surface in the sense of Dirichlet extremality under the TB–Coons constraint.

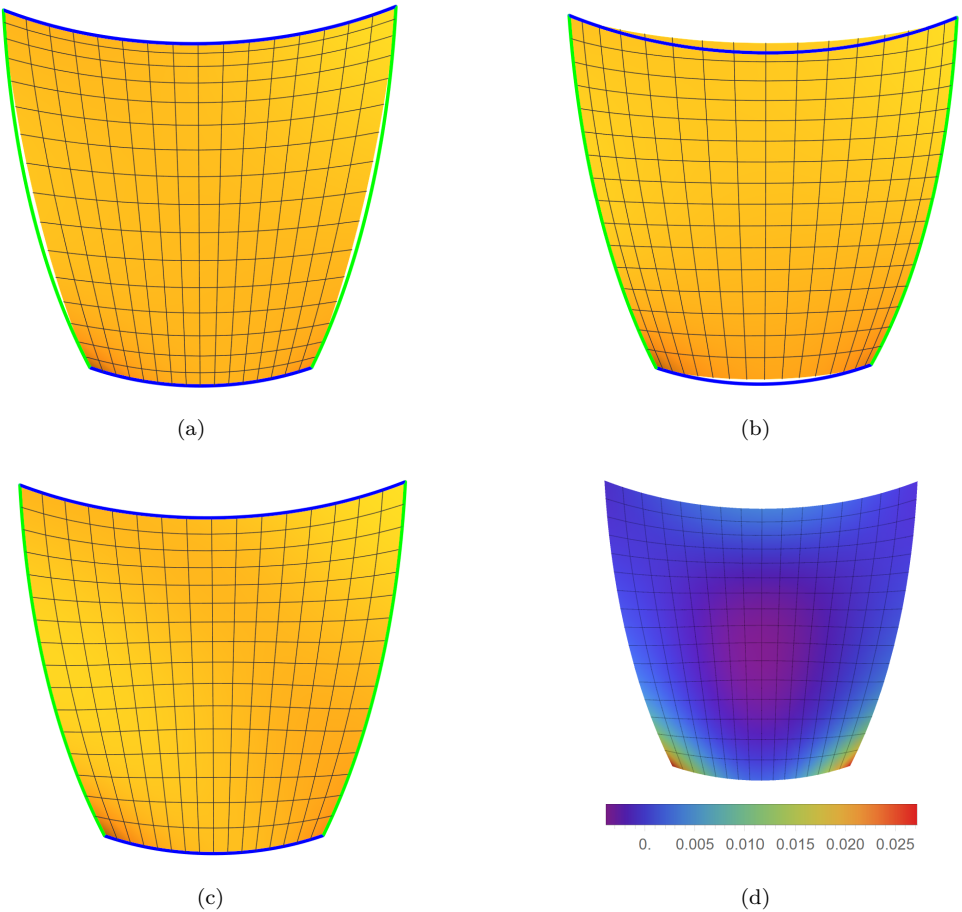


Figure 7: Construction of the TB–Coons surface: (a) R_1 in (7.6), (b) R_2 in (7.7), (c) final surface \mathcal{S} in (7.11), (d) mean curvature nephogram of \mathcal{S} .

8 Conclusion

This work develops a Plateau-type construction for GT-Bézier surfaces by combining harmonic-relaxation ideas with the additional geometric flexibility provided by the generalized trigonometric basis. With boundary interpolation enforced at the level of the control net, the interior degrees of freedom are determined through a Dirichlet-energy extremal condition within the chosen finite-dimensional GT-Bézier space. For each admissible selection of the GT-Bézier basis shape parameters, this variational principle yields a parameter-dependent linear system whose solution specifies the interior control net, and hence a variationally distinguished surface spanning the prescribed boundary data.

A central outcome is a two-level computational strategy: an inner linear solve that produces the Dirichlet extremal surface for fixed parameters, and an outer low-dimensional search that tunes the shape parameters to decrease the Dirichlet energy further. Implemented via particle swarm optimization, this coupling consistently improves the energy in our experiments and, in most tested configurations, leads to a reduction in the realized surface area when compared with classical Bernstein–Bézier Dirichlet patches as well as representative quasi-harmonic and bending-energy competitors, all under identical boundary constraints. The observed improvements support the viewpoint that shape-parameterized non-

polynomial basis can enhance discrete variational surface construction without altering the prescribed boundary geometry.

We also examined the relationship between harmonicity and minimality within this framework. In the unconstrained setting, Dirichlet-energy minimization selects harmonic parametrizations; in contrast, restricting to GT-Bézier tensor-product spaces yields constrained extremals whose deviation from harmonic behavior can be assessed and, when desired, reduced through parameter tuning. Finally, the same extremal Dirichlet principle was transferred to a hybrid TB–Coons construction, providing a systematic way to infer interior control points and generate minimality-biased Coons-type surfaces from sparse boundary information.

Future work includes a sharper analysis of admissible parameter regions and the conditioning of the resulting stiffness systems, the incorporation of explicit conformality measures to strengthen the connection between energy minimization and true area minimization, and extensions to multipatch geometries with continuity constraints and adaptive refinement strategies.

Funding

This research was supported by the Ministry of Higher Education Malaysia through the Fundamental Research Grant Scheme (FRGS/1/2023/STG06/USM/03/04) and by the School of Mathematical Sciences, Universiti Sains Malaysia.

Acknowledgements

The authors are very grateful to the anonymous referees for their valuable suggestions.

A Derivative identities for GT tensor-product patches

This appendix records the derivative identities used in Section 3. Our goal is to justify the “difference-form” representations of the first partial derivatives, which are the key step for separating the integrals and assembling the stiffness coefficients. We keep the presentation compact, but we include the main algebraic steps so that the argument reads as a proof rather than a direct computation.

A.1 Univariate GT-Bézier basis: a derivative recursion

Let $\{G_{k,n}(\cdot; \boldsymbol{\theta})\}_{k=0}^n$ be the univariate GT-Bézier basis generated from the seed (2.3) via the degree-elevation recursion (2.4). Recall the recurrence (with the standard convention $G_{k,n} \equiv 0$ for $k \notin \{0, \dots, n\}$):

$$G_{k,n}(t; \boldsymbol{\theta}) = (1-t)G_{k,n-1}(t; \boldsymbol{\theta}) + tG_{k-1,n-1}(t; \boldsymbol{\theta}). \quad (\text{A.1})$$

Differentiating (A.1) and using the product rule yields, for $n \geq 3$,

$$\begin{aligned} G'_{k,n}(t; \boldsymbol{\theta}) &= \frac{d}{dt} \left((1-t)G_{k,n-1}(t; \boldsymbol{\theta}) \right) + \frac{d}{dt} \left(tG_{k-1,n-1}(t; \boldsymbol{\theta}) \right) \\ &= -G_{k,n-1}(t; \boldsymbol{\theta}) + (1-t)G'_{k,n-1}(t; \boldsymbol{\theta}) + G_{k-1,n-1}(t; \boldsymbol{\theta}) + tG'_{k-1,n-1}(t; \boldsymbol{\theta}), \end{aligned} \quad (\text{A.2})$$

which is the claimed derivative recursion. By iterating (A.2), any $G'_{k,n}$ reduces to the explicit derivatives of the seed functions.

A.2 A univariate “difference form” for GT–Bézier curves

The next lemma is the structural identity used later for surfaces: it rewrites the derivative of a GT curve in terms of first differences of control points plus a lower-degree remainder.

Lemma A.1 (Derivative in difference form). Let $F(t) = \sum_{k=0}^n G_{k,n}(t; \boldsymbol{\theta}) b_k$ be a GT–Bézier curve of degree $n \geq 3$. Then

$$F'(t) = \sum_{k=0}^{n-1} \left(G_{k,n-1}(t; \boldsymbol{\theta}) + t G'_{k,n-1}(t; \boldsymbol{\theta}) \right) (b_{k+1} - b_k) + \sum_{k=0}^{n-1} G'_{k,n-1}(t; \boldsymbol{\theta}) b_k. \quad (\text{A.3})$$

Proof. Differentiate F and insert (A.2):

$$F'(t) = \sum_{k=0}^n G'_{k,n}(t) b_k = \sum_{k=0}^n \left[-G_{k,n-1} + (1-t)G'_{k,n-1} + G_{k-1,n-1} + tG'_{k-1,n-1} \right] b_k.$$

Group the terms into four sums and shift indices in the terms containing $k-1$:

$$\sum_{k=0}^n G_{k-1,n-1} b_k = \sum_{k=0}^{n-1} G_{k,n-1} b_{k+1}, \quad \sum_{k=0}^n t G'_{k-1,n-1} b_k = \sum_{k=0}^{n-1} t G'_{k,n-1} b_{k+1}.$$

Using these shifts (and the convention $G_{n,n-1} \equiv 0$), we obtain

$$F'(t) = \sum_{k=0}^{n-1} \left(G_{k,n-1} + t G'_{k,n-1} \right) (b_{k+1} - b_k) + \sum_{k=0}^{n-1} \left((1-t)G'_{k,n-1} + t G'_{k,n-1} \right) b_k,$$

and the last bracket simplifies to $G'_{k,n-1}$, giving (A.3). \square

A.3 Tensor-product GT–Bézier surface: first partial derivatives

Let S be the GT tensor-product patch (3.2) of bidegree (m, n) :

$$S(u, v; \boldsymbol{\alpha}, \mathbf{P}) = \sum_{i=0}^m \sum_{j=0}^n P_{ij} G_{i,m}(u; \boldsymbol{\alpha}^{(u)}) G_{j,n}(v; \boldsymbol{\alpha}^{(v)}).$$

Termwise differentiation immediately gives the separated representations

$$\begin{aligned} S_u(u, v) &= \sum_{i=0}^m \sum_{j=0}^n P_{ij} G'_{i,m}(u; \boldsymbol{\alpha}^{(u)}) G_{j,n}(v; \boldsymbol{\alpha}^{(v)}), \\ S_v(u, v) &= \sum_{i=0}^m \sum_{j=0}^n P_{ij} G_{i,m}(u; \boldsymbol{\alpha}^{(u)}) G'_{j,n}(v; \boldsymbol{\alpha}^{(v)}), \end{aligned} \quad (\text{A.4})$$

where G' can be evaluated using (A.2).

A.4 Difference-form representations for S_u and S_v

For assembling the normal equations in Section 3, it is useful to isolate first differences of control points in the u - and v -directions. This follows by applying Lemma A.1 in one parameter while treating the other parameter as a spectator.

Fix v and define a u -curve with v -dependent control points

$$B_i(v) := \sum_{j=0}^n P_{ij} G_{j,n}(v; \boldsymbol{\alpha}^{(v)}), \quad \text{so that} \quad S(u, v) = \sum_{i=0}^m G_{i,m}(u; \boldsymbol{\alpha}^{(u)}) B_i(v).$$

Applying Lemma A.1 to the curve $u \mapsto S(u, v)$ yields

$$S_u(u, v) = \sum_{i=0}^{m-1} \left(G_{i,m-1}(u) + u G'_{i,m-1}(u) \right) (B_{i+1}(v) - B_i(v)) + \sum_{i=0}^{m-1} G'_{i,m-1}(u) B_i(v), \quad (\text{A.5})$$

where, for readability, we suppressed the parameter vectors in $G_{i,\cdot}(\cdot; \boldsymbol{\alpha}^{(u)})$. Expanding $B_{i+1}(v) - B_i(v)$ and $B_i(v)$ in terms of the surface control points gives

$$\begin{aligned} S_u(u, v) &= \sum_{i=0}^{m-1} \sum_{j=0}^n \left(G_{i,m-1}(u; \boldsymbol{\alpha}^{(u)}) + u G'_{i,m-1}(u; \boldsymbol{\alpha}^{(u)}) \right) G_{j,n}(v; \boldsymbol{\alpha}^{(v)}) (P_{i+1,j} - P_{i,j}) \\ &\quad + \sum_{i=0}^{m-1} \sum_{j=0}^n G'_{i,m-1}(u; \boldsymbol{\alpha}^{(u)}) G_{j,n}(v; \boldsymbol{\alpha}^{(v)}) P_{i,j}. \end{aligned} \quad (\text{A.6})$$

The formula for S_v is obtained analogously by fixing u and applying Lemma A.1 to the v -direction, which yields

$$\begin{aligned} S_v(u, v) &= \sum_{i=0}^m \sum_{j=0}^{n-1} G_{i,m}(u; \boldsymbol{\alpha}^{(u)}) \left(G_{j,n-1}(v; \boldsymbol{\alpha}^{(v)}) + v G'_{j,n-1}(v; \boldsymbol{\alpha}^{(v)}) \right) (P_{i,j+1} - P_{i,j}) \\ &\quad + \sum_{i=0}^m \sum_{j=0}^{n-1} G_{i,m}(u; \boldsymbol{\alpha}^{(u)}) G'_{j,n-1}(v; \boldsymbol{\alpha}^{(v)}) P_{i,j}. \end{aligned} \quad (\text{A.7})$$

Formulas (A.6)–(A.7) are exactly the representations invoked in Section 3 to separate the integrals and form the stiffness coefficients (3.5)–(3.8).

References

- [1] Antonio Alarcón, Franc Forstnerič, and Francisco J López. Minimal surfaces from a complex analytic viewpoint, volume 10. Springer, 2021.
- [2] Juan Monterde. Bézier surfaces of minimal area: The Dirichlet approach. *Computer Aided Geometric Design*, 21(2):117–136, 2004.
- [3] Sebastian Kapfer, Stephen Hyde, Klaus Mecke, Christoph Arns, and Gerd Schröder-Turk. Minimal surface scaffold designs for tissue engineering. *Biomaterials*, 32(29):6875–6882, 2011.
- [4] Benjamin Andrew Burton. Minimal triangulations and normal surfaces. University of Melbourne, Department of Mathematics and Statistics, 2003.
- [5] Tobias Colding and William Minicozzi. A course in minimal surfaces, volume 121. American Mathematical Soc., 2011.
- [6] Ulrich Dierkes, Stefan Hildebrandt, Albrecht Küster, and Ortwin Wohlrab. Minimal surfaces. In *Minimal Surfaces I: Boundary Value Problems*, pages 53–88. Springer, 2010.

- [7] Øystein Tråsdahl and Einar Rønquist. High order numerical approximation of minimal surfaces. *Journal of Computational Physics*, 230(12):4795–4810, 2011.
- [8] Dong-Jin Yoo. Computer-aided porous scaffold design for tissue engineering using triply periodic minimal surfaces. *International Journal of Precision Engineering and Manufacturing*, 12:61–71, 2011.
- [9] Qing Pan and Guoliang Xu. Construction of minimal subdivision surface with a given boundary. *Computer-Aided Design*, 43(4):374–380, 2011.
- [10] Yan Wang. Periodic surface modeling for computer aided nano design. *Computer-Aided Design*, 39(3):179–189, 2007.
- [11] Jesse Douglas. Solution of the problem of plateau. *Transactions of the American Mathematical Society*, 33(1):263–321, 1931.
- [12] Tobias Colding and William P Minicozzi. Minimal surfaces and mean curvature flow. arXiv preprint arXiv:1102.1411, 2011.
- [13] Keenan Crane, Fernando De Goes, Mathieu Desbrun, and Peter Schröder. Digital geometry processing with discrete exterior calculus. In *ACM SIGGRAPH 2013 Courses*, pages 1–126. 2013.
- [14] Robert Osserman. *A survey of minimal surfaces*. Courier Corporation, 2013.
- [15] Juan Monterde. The plateau-Bézier problem. In *Mathematics of Surfaces: 10th IMA International Conference*, Leeds, UK, September 15–17, 2003. *Proceedings*, pages 262–273. Springer, 2003.
- [16] Yong-Xia Hao, Ren-Hong Wang, and Chong-Jun Li. Minimal quasi-Bézier surface. *Applied Mathematical Modelling*, 36(12):5751–5757, 2012.
- [17] John Barrett, Harald Garcke, and Robert Nürnberg. A parametric finite element method for fourth order geometric evolution equations. *Journal of Computational Physics*, 222(1):441–467, 2007.
- [18] Yong-Xia Hao, Chong-Jun Li, and Ren-Hong Wang. An approximation method based on MRA for the quasi-plateau problem. *BIT Numerical Mathematics*, 53(2):411–442, 2013.
- [19] Konrad Polthier. Polyhedral surfaces of constant mean curvature. PhD thesis, *Habilitationsschrift* TU Berlin, 2002.
- [20] Keenan Crane. Discrete differential geometry: An applied introduction. *Notices of the AMS*, Communication, 1153, 2018.
- [21] Patrick Mullen, Yiyi Tong, Pierre Alliez, and Mathieu Desbrun. Spectral conformal parameterization. In *Computer Graphics Forum*, volume 27, pages 1487–1494. Wiley Online Library, 2008.
- [22] Mei-Heng Yueh, Wen-Wei Lin, Chin-Tien Wu, and Shing-Tung Yau. An efficient energy minimization for conformal parameterizations. *Journal of Scientific Computing*, 73(1):203–227, 2017.
- [23] Qing Pan and Guoliang Xu. Construction of minimal subdivision surface with a given boundary. *Computer-Aided Design*, 43(4):374–380, 2011.
- [24] Gang Xu and Guo-zhao Wang. Quintic parametric polynomial minimal surfaces and their properties. *Differential Geometry and its Applications*, 28(6):697–704, 2010.

[25] Gang Xu and Guozhao Wang. Parametric polynomial minimal surfaces of degree six with isothermal parameter. In *Advances in Geometric Modeling and Processing: 5th International Conference, GMP 2008, Hangzhou, China, April 23-25, 2008. Proceedings* 5, pages 329–343. Springer, 2008.

[26] Geng Li, Jin-Fu Chen, CP Sun, and Hui Dong. Geodesic path for the minimal energy cost in shortcuts to isothermality. *Physical Review Letters*, 128(23):230603, 2022.

[27] Ognian Kassabov. Transition to canonical principal parameters on minimal surfaces. *Computer Aided Geometric Design*, 31(7-8):441–450, 2014.

[28] Daud Ahmad and Bilal Masud. Variational minimization on string-rearrangement surfaces, illustrated by an analysis of the bilinear interpolation. *Applied Mathematics and Computation*, 233:72–84, 2014.

[29] Muhammad Ammad, Md Yushalify Misro, and Ahmad Ramlı. A novel generalized trigonometric Bézier curve: properties, continuity conditions and applications to the curve modeling. *Mathematics and Computers in Simulation*, 194:744–763, 2022.

[30] Ahmed Gad. Particle swarm optimization algorithm and its applications: A systematic review. *Archives of computational methods in engineering*, 29(5), 2022.

[31] Tareq Shami, Ayman El-Saleh, Mohammed Alswaitti, Qasem Al-Tashi, Mhd Amen Summakieh, and Seyedali Mirjalili. Particle swarm optimization: A comprehensive survey. *Ieee Access*, 10:10031–10061, 2022.

[32] Yong-Xia Hao. Quasi-area functional for the Plateau–Bézier problem. *Graphical Models*, 112:101095, 2020.

[33] Wai Yeung Lam. Discrete minimal surfaces: critical points of the area functional from integrable systems. *International Mathematics Research Notices*, 2018(6):1808–1845, 2018.

[34] Daud Ahmad, M Khalid Mahmood, Qin Xin, Ferdous MO Tawfiq, Sadia Bashir, and Arsha Khalid. A computational model for q-Bernstein quasi-minimal bézier surface. *Journal of Mathematics*, 2022(1):8994112, 2022.

[35] Rida Farouki. The Bernstein polynomial basis: A centennial retrospective. *Computer Aided Geometric Design*, 29(6):379–419, 2012.

[36] George Phillips. *Interpolation and approximation by polynomials*, volume 14. Springer Science & Business Media, 2003.

[37] Gerald Farin. *Curves and surfaces for computer-aided geometric design: a practical guide*. Elsevier, 2014.

[38] Janmenjoy Nayak, Swapnarekha, Bighnaraj Naik, Gaurav Dhiman, and Vimal. 25 years of particle swarm optimization: Flourishing voyage of two decades. *Archives of Computational Methods in Engineering*, 30(3):1663–1725, 2023.

[39] Dongshu Wang, Dapei Tan, and Lei Liu. Particle swarm optimization algorithm: an overview. *Soft computing*, 22(2):387–408, 2018.

- [40] Meetu Jain, Vibha Sailjpal, Narinder Singh, and Satya Bir Singh. An overview of variants and advancements of PSO algorithm. *Applied Sciences*, 12(17):8392, 2022.
- [41] Yudong Zhang, Shuihua Wang, and Genlin Ji. A comprehensive survey on particle swarm optimization algorithm and its applications. *Mathematical problems in engineering*, 2015(1):931256, 2015.
- [42] Yongwei Miao, Huahao Shou, Jieqing Feng, Qunsheng Peng, and A Robin Forrest. Bézier surfaces of minimal internal energy. In *Mathematics of Surfaces XI: 11th IMA International Conference, Loughborough, UK, September 5-7, 2005. Proceedings*, pages 318–335. Springer, 2005.